Available online at www.sciencedirect.com
SCIENCE DIRECT
Journal of Molecular Graphics and Modelling 24 (2005) 111–120
Journal of Molecular Graphics and Modelling
www.elsevier.com/locate/JMGM

Rendering of quantum topological atoms and bonds

M. Rafat, M. Devereux, P.L.A. Popelier *

School of Chemistry, Sackville Site, University of Manchester, Manchester M60 1QD, UK

Accepted 4 May 2005
Available online 20 June 2005

Abstract

In this article, we describe and apply an algorithm that visualizes atoms and bonds in molecules and van der Waals complexes, based on the topology of the electron density. The theory of quantum chemical topology defines both atoms and bonds via a single consistent procedure, and enables the association of an atomic shape with an atomic property (charge, dipole moment, volume, ...). Special attention is paid to the bridging of gaps arising in interatomic surfaces, in the presence of ring critical points or high ellipticity. This algorithm, in conjunction with the graphical user interface of the computer program MORPHY enables robust and efficient rendering of complicated interatomic surfaces, as found in larger systems.

Keywords: Electron density; Quantum chemical topology; Atoms; Bonds; Graphical user interface; Interatomic surface; Atoms in molecules

1. Introduction

Visual representations of atoms and bonds are important tools in chemical research and scientific progress in general. Three-dimensional ball-and-stick models, used alongside flexible graphical user interfaces, provide insight in complex molecules and crystalline materials. Molecular simulations benefit too from images that enable the rapid analysis of intricate structural details. Of course, prior to any such visualization one must first decide what atoms and bonds really are. Although this question seems innocuous, and its answer taken for granted by many, it is still under debate (e.g. [1] and references therein and particularly [2–4]).

Atomic properties can be obtained [5] via three classes of methods: partitioning of orbital space, partitioning of the Hamiltonian and partitioning of the electron density. The first class encompasses popular population analyses such as Mulliken's and Natural Population Analysis. Although these methods supply atomic charges they do not provide a concomitant picture of the atom's shape. In other words, the atomic property is severed from the atom's visual representation. Similarly, distributed multipole analysis (DMA), which also belongs to the first class of methods, allocates high-order multipole moments to atomic sites, again without providing a visual representation of the atom. The second class of methods poses the even more fundamental, if not impossible, challenge of wedding an atom's (physical) property to its picture. *Only the third class, which involves the electron density, provides a natural path to achieve this aim*. Moreover, the electron density, performing a central role in density functional theory, acts as a convenient information ''platform'' where experiment meets theory. A variety of computational schemes all yield the electron density at some point, regardless of the type of basis function (if present) or the way they tackle electron correlation, for example. It is therefore desirable that one's definition of an atom and a bond depends directly on the electron density itself, rather than on the features of the scheme by which the electron density was obtained. To give a simple example, the concept of a Mulliken charge ceases to exist when using plane-wave basis functions because such basis functions are not centered on nuclear positions.

We propose the topology of the electron density as a starting point to define an atom and a bond. Not only do they both follow from the same topological analysis, in a computable manner, but they also associate pictures of atomic shapes with atomic properties. Indeed, one can associate the well-defined bounded region in three-dimensional space occupied by a topological atom with its

* Corresponding author. Tel.: +44 161 3064511; fax: +44 161 3064559.
E-mail address: pla@manchester.ac.uk (P.L.A. Popelier).

1093-3263/$ – see front matter © 2005 Elsevier Inc. All rights reserved.
doi:10.1016/j.jmgm.2005.05.004

multipole moments. In addition, the quantum chemical topology (QCT) [6–11] approach is rooted [12] in quantum mechanics via Schwinger's quantum action principle, which was taken as a natural starting point to generalize quantum mechanics to subspace quantum mechanics.

In summary, *QCT enjoys the benefit of visual representation going hand in hand with physical property*, and the benefit that it is based on the electron density itself, rather than on the way it was obtained. However, this accomplishment is overshadowed by the computational time and intricacy posed by the algorithms that generate topological atoms and bonds. Nevertheless, substantial progress has been made by various groups. The program EVolVis [13], for example, enables the user to interactively explore a molecule's electron density for topological features. The popular electron localization function (ELF) [14] is also regularly subject to a visual analysis [15–18], while high-resolution X-ray electron density can be analyzed via the program TOPXD [19] and crystalline materials via TESSEL [20].

That there is a need to visualize molecules is clearly demonstrated by the popularity of molecular surfaces, such as the Corey–Pauling–Koltun (CPK) [21] surfaces and solvent accessible surfaces [22]. The method presented here is able to carve a molecule out of a supermolecular cluster, since according to QCT a molecule is simply a union of non-overlapping and space-exhausting atoms. The need for visualization is straightforwardly extended from molecules to atoms. For example, the small volume of sp^3 carbons [23] can be understood in terms of a simple picture, and so is the formation of spikes in the Li^+ cation in the rock-salt phase of the LiF crystal [24]. The curvature of the boundaries of topological atoms (i.e. interatomic surfaces) has also been related to atomic hardness by an in-depth study [25] based on work [26] pioneering the use of differential geometry in QCT. Communicating the meaning of topological atoms via pictures instead of mathematical descriptions is very direct. On the ''technical'' front, being able to visualize atoms is simply vital in the design of correct and robust algorithms for integration over topological subspaces or basins.

Perhaps contrary to some readers' expectations we do *not* investigate the issue of transferability in this paper. In fact, we believe it to be imprudent, if not wrong, to assess transferability on the basis of visual information alone. To make this point more acute, one should visually compare the actual molecular electron density and the corresponding promolecular electron density. The latter is a simple superposition of spherically averaged and unhybridized atomic electron densities. Visually, the promolecular density is virtually identical to the real one, which leaves one with the false impression that the physical properties (e.g. energy, dipole moments) associated with both densities would also be virtually identical. If this were true, then there would be no need to keep developing faster and more accurate ab initio quantum chemistry algorithms and packages. The MEDLA approach [27] is an example of a visual assessment of transferability.

In this article, we present a new algorithm that generates smooth interatomic surfaces (or zero-flux surfaces), without gaps and in complex topological situations. This accomplishment required much careful thought and development. The applications shown are subject to the illustration of the algorithm although they have interest in their own right. We also aim at handling larger systems than typically published so far. When combined with the current power of Java-based graphical user interface (GUI) tools (including the non-standard Java3D extension to enable 3D graphics), we hope to have furthered the frontier of topological visualization.

2. The algorithm

2.1. Problem description

An interatomic surface (IAS) is a bundle of gradient paths (GPs) originating at infinity and attracted to a bond critical point (BCP). A GP is a path of steepest ascent through the electron density and a BCP is a type of saddle point marking the boundary between two atoms, together with the IAS. The IAS constitutes a sharp boundary between two topological atoms.

The first step in the representation of IASs is obtaining sample points on the whole surface. This is easily achieved by tracing GPs *backwards* (i.e. in the direction of steepest descent), starting from a small circle centered at the BCP and proceeding towards infinity. This small circle contains a number of equidistant points from which the GPs start their journey. Sample points (yellow points in Fig. 1) are then collected at regular intervals on the GPs. However, these points often do not represent the complete IAS, because two originally adjacent GPs may wander off in increasingly different directions, leaving a gap in the IAS. One of the main challenges of a robust surface representation algorithm is to bridge such gaps efficiently. These gaps can have two origins.

One possibility is that the gap is caused by a high ellipticity at the BCP. The ellipticity essentially measures the ratio of two local curvatures in the electron density, each one in a direction orthogonal to the other, and both describing the orientation of a plane tangent to the IAS. A high ellipticity means that a GP advances much faster in one direction than in the other, as shown in Fig. 1. Here, the vertical direction dominates the horizontal one; as the GPs take off from their initial points, equidistantly spaced on a small circle, they are immediately pulled in the vertical direction. This effect creates two enormous gaps at the left-hand side of the picture.

The other possible cause for the appearance of a gap is the presence of a ring critical point (RCP) inside the IAS. An RCP is the other possible type of saddle point, so called because it emerges inside a ring of topologically connected nuclei. An RCP suddenly alters the direction of certain GPs of the IAS as they approach the RCP. This is shown in Fig. 1

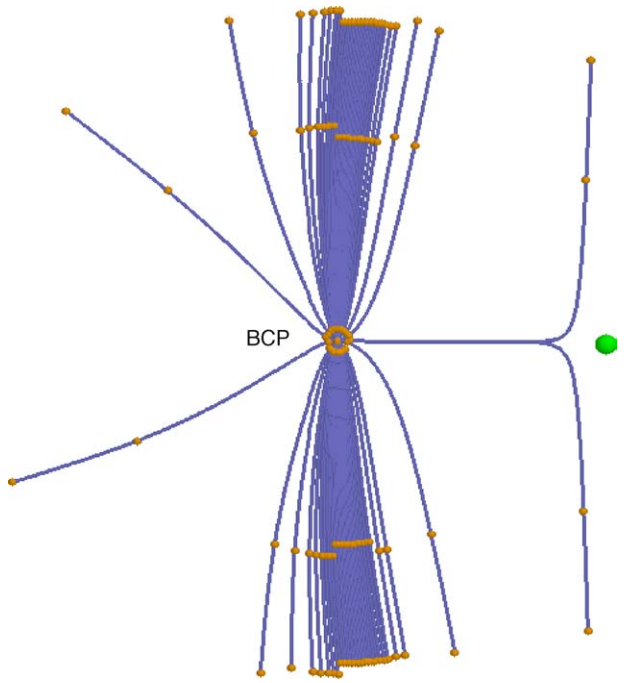

Fig. 1. Example of gaps inside a surface. The gradient paths (blue) are traced from a circle around the bond critical point (BCP). The high ellipticity means that the paths are not evenly distributed, leaving large parts of the surface unexplored. The presence of a ring critical point (RCP) (green) accentuates the unequal distribution of the paths.

at the right-hand side, where two adjacent GPs paths approach the RCP from the same direction and in the immediate vicinity of the RCP one GP proceeds upwards and the other downwards.

The gap problem is well known and has plagued the development of atomic integration algorithms. For example, the first useful integration algorithm, which was designed by Biegler-König et al. [28] and implemented in AIMPAC under the name of PROAIM, suffered from erroneous integration results due to gaps. They cause a topological atom to be locally unbounded, which explains why some integration rays of the Gauss–Legendre quadrature simply shoot through the IAS. In response to this serious shortcoming Keith modified PROAIM's source code by adding an integration algorithm that avoids an explicit knowledge of an IAS's location. This algorithm determines in which topological atom a given point in space is lying. This is an expensive procedure because a GP must be traced from this point to the path's attractor, which is usually the nucleus of the atom that houses the point. The idea is also the basis for the "non-analytical" integration algorithm [29] in MORPHY98 and the "octree" algorithm [30], which delineates topological basins in an arbitrary three-dimensional quantum mechanical density function. Since the algorithm presented in this paper solves the gap problem it restores the availability of an *explicit* IAS, defined everywhere. As a result it enables a more robust atomic integration algorithm, one which avoids the expensive GP tracing required to find attractors. However, this work will be reported on in more detail elsewhere.

2.2. Algorithm outline

Since the two kinds of gap are very different in nature they need separate treatment. If high ellipticity is the cause then one should add extra points, otherwise large parts of the basin will remain unexplored. If an RCP is the cause then adding extra points will not solve the problem; on the contrary, we could mistakenly step into another atom if the points are not added carefully, as explained below (Section 2.2.4).

2.2.1. Growth of the interatomic surface

As shown in Fig. 2a, we 'grow' the IAS from a very small circle of initial points around the BCP. In other words, we trace the GPs from these initial points and record points in the IAS each time the GP tracing is halted. The GPs are stopped whenever the electron density reaches predetermined contour values, that is, at "*iso-density*" contours. A representative atom is bounded by more than one IAS, each one corresponding to a BCP. The starting value of the set of iso-density contours is that of the BCP with the highest electron density. The electron density is reduced by a (user-defined) factor between 1.3 and 1.1 (for very smooth IASs) from one contour to the next, such that an IAS is typically modeled by 10–50 iso-density contours. We construct the surface by triangulation of the points that embody it. As a consequence of the path tracing method the points roughly follow the iso-density contours. Hence, it is natural to define a '*growth level*' as the set of points on the same contour. The electron density value of the iso-density contour line is customized to each atom and it depends on the concentration of the points on the initial circle around each BCP.

2.2.2. Connection of points on the interatomic surface

Once we have obtained the points covering the surface we triangulate them. The simplest way is to use an 'automatic triangulation' scheme, which produces the same connection

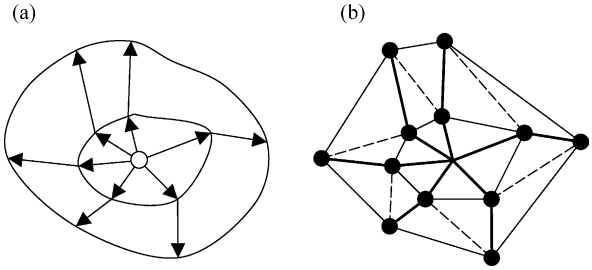

Fig. 2. (a) Gradient paths (arrows) and iso-density contours. The gradient paths start in a small circle around the bond critical point and are stopped at predetermined contour values of constant electron density. At every contour value new points are recorded and used for the triangulation of the interatomic surface. (b) Triangulation of the surface. The gradient paths (bold) and growth levels (plain lines) are used as a guide for the triangulation, which is completed with the dashed lines.

pattern for the whole surface. However, this scheme is not very flexible because if one point is deleted then the triangulation has to be totally reorganized. Moreover, it is not straightforward to add new points to the surface after it has been triangulated. An alternative way to retrieve the surface is the Delaunay triangulation method [31]. This method enables the triangulation of a set of points on the basis of geometrical criteria only. It is highly flexible as one can add or delete points and triangulate the object at the end, once all the points are located. Other advantages of the Delaunay triangulation are its uniqueness and its optimal "equi-angularity" (i.e. it avoids long and/or thin triangles). Although the method was initially developed for 2D or 3D convex objects, it is also possible to triangulate surfaces [32] and objects of an arbitrary shape [33,34]. However, the Delaunay method is not chemically intuitive since it disregards the way in which the IAS was grown. This method ruthlessly connects points in an attempt to increase the equi-angularity, thereby destroying connections that reflect the history of the IAS's growth. The lack of natural connections and the computational overhead associated with the equi-angularity (which is an irrelevant property for our purposes) made us return to the automatic triangulation.

There are two important rules that govern this type of triangulation. They are illustrated in Fig. 2b. Firstly, points from adjacent iso-density contours are connected (by bold lines), provided they lie along a given GP. Secondly, two adjacent points on the same iso-density contour are connected (by solid thin lines). This connection is referred to as a *segment*. This rule causes a sequence of segments to follow the smooth contour lines shown in Fig. 2a. The combined rules create a pattern of quadrilaterals, each of which needs to be cut in two triangles in order to complete the triangulation. This is done by connecting two subsequent iso-density levels (dashed lines). There are always two possible ways to cut a quadrilateral in two triangles. One way was arbitrarily selected beforehand and then systematically implemented by the algorithm. This method of triangulation is very quick and also chemically intuitive. Indeed the connections follow the GPs and the iso-density contour lines. The drawback of this method is the lack of flexibility. We cannot easily delete a point and therefore regions with a very high concentration of points may appear, for instance if the ellipticity is high.

2.2.3. Adding midpoints

In order to avoid missing large parts of the IAS, we add a point in the middle of a segment of a given growth level if the segment becomes too long. This course of action is illustrated in Fig. 3. Each newly added midpoint is the origin of a new GP. This action contributes substantially to the success of the algorithm in finding the whole IAS in the presence of high ellipticity. It should be pointed out that there is no guarantee that the added midpoints rigorously lie in the IAS. However, if the surface is locally flat the segment can be regarded as lying in the IAS. Nevertheless, if the IAS has strong local curvature this approximation can create a small error in the representation of the surface. A second point to make here is no midpoints are added within a reasonably large neighbourhood of an RCP, for reasons explained in the next section.

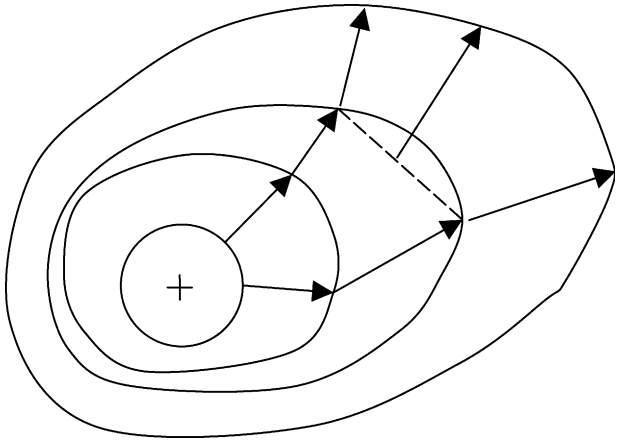

Fig. 3. Addition of a midpoint: when two gradient paths (arrows) become separated by a large distance (dashed line) then a midpoint is added and grown until the next level. The circles represent the iso-density contours and the cross represents the bond critical point.

It should be emphasized that simply adding more initial points on the small circle around the BCP does not solve the problem of gaps in the case of high ellipticities. Even if the points are chosen judiciously, by varying their density or replacing the circle by an appropriately orientated and proportioned ellipse, no progress is made. The drawback prompted the design [29] of the robust but expensive "non-analytical" integration algorithm, in which no explicit knowledge of an IASs is required. This shows again the great potential of the current IAS representation to drive atomic integration and present a cheaper and equally robust alternative.

2.2.4. Ring critical point and ring line

The presence of an RCP has a dramatic effect on the growth of an IAS because the RCP makes the bundle of GPs forming the IAS diverge in two opposite directions. This "tearing effect" occurs at either side of a unique GP that connects the BCP to the RCP. This GP is shown as a dotted line in Fig. 4. If this path intersects the JK segment then J and K will grow apart in two different directions creating a gap in the IAS. Adding midpoints does not solve this problem. Extra GPs originating in these midpoints (inserted between J′ and K′) do not reach the gap either. The solution would be to add the ring line and the RCP to the surface (a ring line consists of two GPs, originating at infinity and being attracted to the RCP). Unfortunately, this unique GP is often expensive and difficult to locate, which is why the current algorithm avoids this task. Instead, we only have access to the positions of all RCPs, which are located beforehand. During the triangulation, the algorithm detects which surface contains an RCP and is

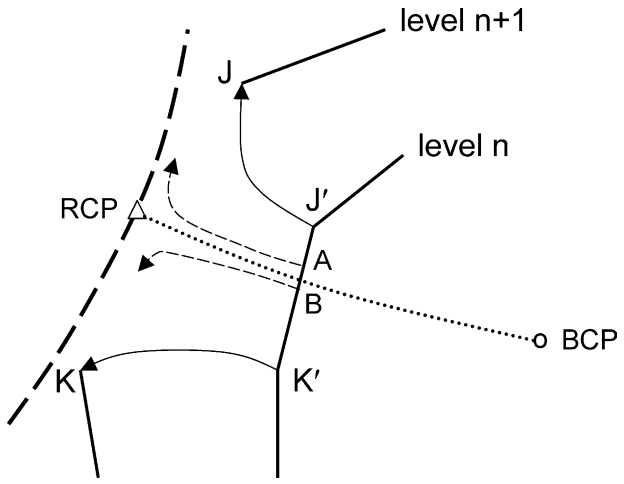

Fig. 4. Detection of a ring critical point (triangle) in an interatomic surface. The arrows (plain and dashed) represent traced gradient paths. The bold plain lines represent the growth levels, the dashed line the ring line and the dotted line the gradient path connecting the bond critical point (BCP) and ring critical point (RCP). The ring critical point is confirmed as lying on the segment J–K if the paths from A and B approach the ring critical point very closely.

thus in a position to modify the triangulation's connections accordingly. Since the value of the electronic density at the RCP is known, we can predict between which two iso-density contours it will appear.

Fig. 4 shows two sequential iso-density contours in the presence of an RCP. We first focus on how the RCP affects the IAS. The RCP deflects GPs in two opposite directions, which invalidates the establishment of a segment connecting point J and K. Several tests are required to determine the location of such points J and K. Chronologically, they are (with an eye on Fig. 4):

- J′ and K′ must be close enough to the RCP.
- The RCP must lie in between the points J and K, which is determined via a geometrical (rather than topological) test.
- In preparation of this test, a bisection algorithm searches for two points A and B (on the J′–K′ segment at level n), lying as close as possible to each other (below a given threshold) and such that a GP through point A is deflected upwards and a GP through point B downwards. The test demands that these two differently deflected GPs come close enough to the RCP.

The last step ensures that the directional divergence of the GP is actually due to the RCP. This test is obviously the most expensive one but the first two tests guarantee that only a handful of suspicious connections filter through to the last step.

Multiple RCPs occurring in one IAS are fairly common and hence the algorithm should also be able to handle this. During the IAS's growth (outwards from the BCP) the algorithm decides if an RCP, drawn from a list of candidates, is potentially part of the IAS. The decision is positive if any point of the IAS lies close enough to the RCP. If a gap is detected then the algorithm applies the three tests to the list of RCPs that are considered as being part of the IAS.

We now comment on the final step in the construction of a triangulated IAS, which is to add a ring line to the IAS. When the RCP has been found to lie in between the points J and K, these two points will have a special status in the surface: they are the origin of the *border* of the IAS. This border is to be regarded as an outside edge. These two points J and K and the points located further along the GPs running through them constitute the outer edge of the IAS. In other words, no other points generated in the triangulation procedure will come closer to the ring line. It is also important to note that no midpoints will ever be added between the two GPs, one through J and one through K. A ring line is part of an IAS and needs to be included. However, the GPs traced from the initial circle can only approach it asymptotically close. Therefore, they cannot be used to trace the ring line. This is why points on the ring line have to be added separately as part of the IAS. If not, the IAS will never reach the ring line and will therefore not be complete. The last step is then to grow the ring line itself (which is trivial) and connect it to the border of the IAS. As soon as the RCP is detected the border of the IAS is known. It is just a matter of connecting with triangles the growth levels of the border of the IAS and the ring line.

2.2.5. Cage critical points

A cage critical point is a minimum in the electron density. Since it is *not* a saddle point it does not abruptly change the direction of GPs in its immediate vicinity; in fact, a cage critical point does not deflect GPs at all, i.e. it does not induce strong local curvatures. Its topological effect on an IAS is to attract and sink all the GPs around it, provided one traces the GPs in the opposite direction (i.e. as paths of steepest descent). Locally, a cage critical point makes triangles near it shrink into one point. However, in the vicinity of the cage critical the IAS can still be described by triangles. Hence, no special treatment is required.

For convenience, the whole algorithm is summarized in the flowchart shown in Fig. 5.

3. Applications

In this section, we show a series of examples spanning a variety of molecules and complexes, often of substantial topological complexity. The IASs terminate at different contour values, decided on merely esthetic grounds. The values of the electron density (in atomic units) are: diborane (0.0005), hydrated magnesium ion (0.0005), [18]annulene (0.0005), adamantane (0.0005), water nonamer (0.0001), ferrocene (0.001), tuftsin (0.001) and CpG (0.0001).

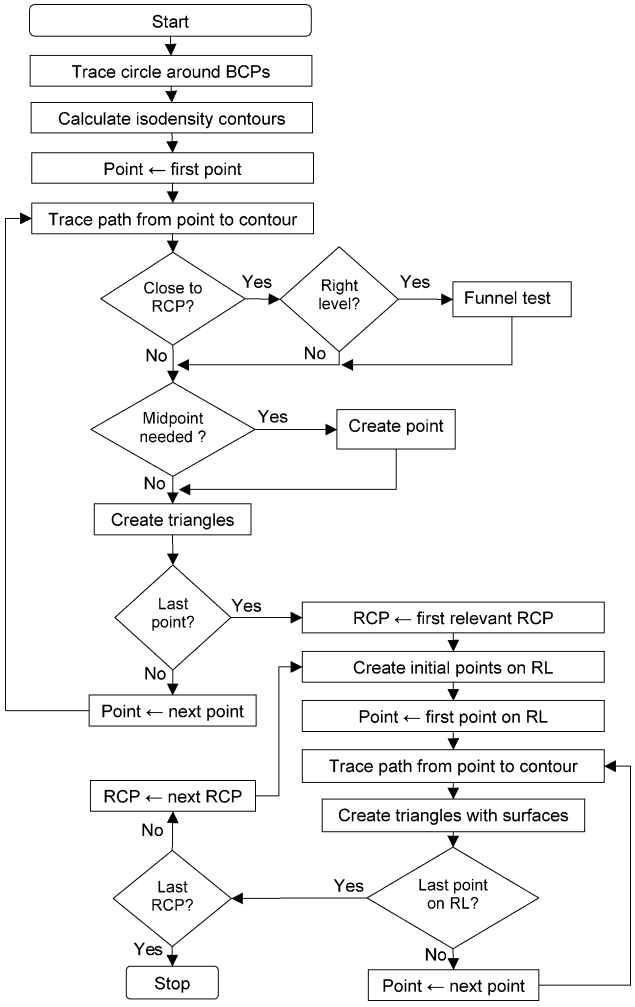

Fig. 5. Algorithm flowchart. For abbreviations, see text, RL: ring line. Reverse arrow in $A \leftarrow B$ indicates that variable A adopts the value of variable B.

3.1. Diborane

Fig. 6 shows the boron atom in diborane (B_2H_6). This atom is bounded by four IASs, each one constituting a boundary between it and one of four neighbouring hydrogen atoms. The two borons form a four-membered ring with the two hydrogens, based on their topological connectivity as expressed by the bond paths (a bond path is the collection of two GPs that originate at a BCP and are attracted to two bonded nuclei). This connection creates a ring critical point, which is contained in the two IASs (above and below) on the right of the picture. Moreover, these two IASs are each associated with a BCP that displays a high ellipticity ($\varepsilon = 0.61$). So, these IASs are particularly interesting and challenging since they include the two kinds of gap. It is clear that after triangulation we are able to retrieve the whole IASs, due to the addition of midpoints. The RCP was correctly diagnosed as being part of the IASs and the ring line has been added explicitly. This line runs perpendicular to the plotting plane and accentuates the cusp like nature of the topological atom.

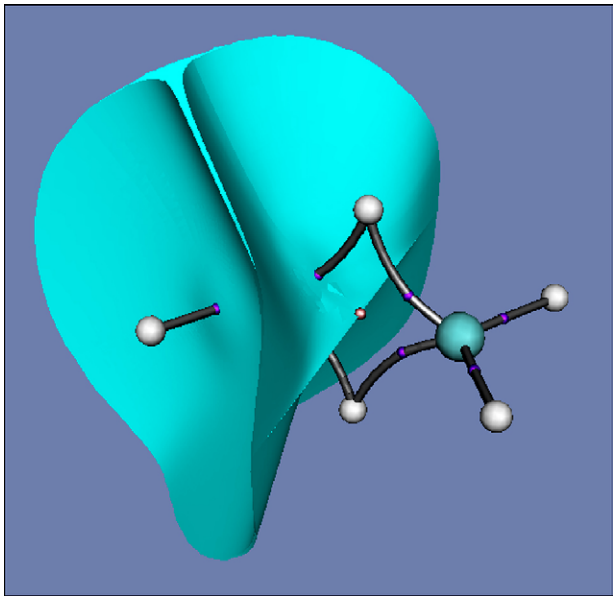

Fig. 6. The boron atom in B_2H_6. The boron nuclei (blue) and the hydrogen nuclei (white) are linked by bond paths (grey). The bond critical points are marked in purple and the ring critical point in pink.

3.2. Hydrated magnesium ion

Solvated ions are interesting to study from the point of view of QCT because their short-range polarization can be linked with the way the surrounding solvent molecules change their shape. Fig. 7 shows a penta-hydrated

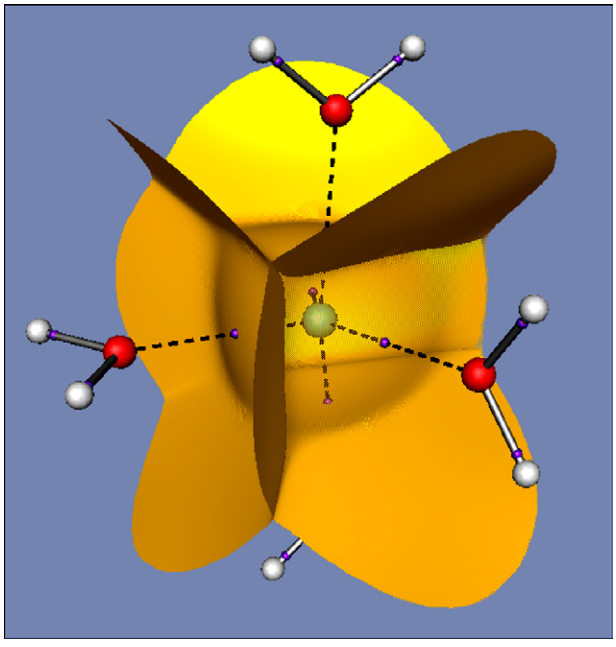

Fig. 7. A penta-hydrated Mg ion, $[Mg(H_2O)_5]^{2+}$. All interatomic surfaces are marked in solid orange except the semi-transparent interatomic surface separating the Mg from the water molecule at the right. Covalent bond paths (plain grey) connect the oxygens (red) and the hydrogens (white). Non-covalent bond paths are marked as black dashed lines. The bond critical points, appearing in the center of the interatomic surfaces are shown in purple.

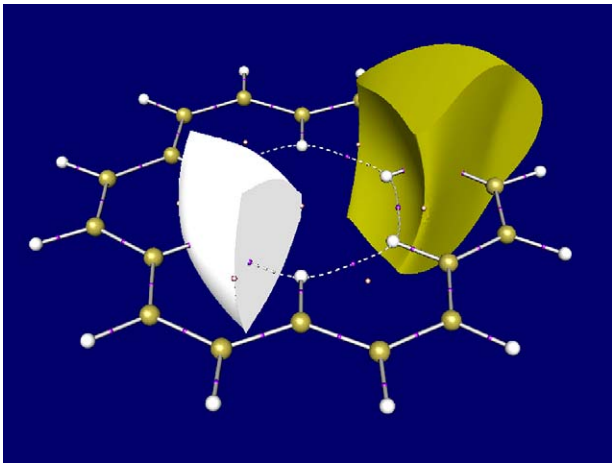

Fig. 8. A carbon (gold) and a hydrogen (white) atom in [18]annulene. Covalent bond paths are marked by grey solid lines and the non-covalent one by white dashed lines. The bond critical points are shown in purple and the ring critical points in pink.

magnesium ion as an example. Topologically, this example is easy since there are no RCP in the complex and the ellipticitiy of all Mg–O bond critical points is low. The GUI automatically differentiates covalent and non-covalent bond paths by a simple distance criterion. This attribute makes the rendering clearer but a more sophisticated criterion based on electronic information is probably warranted. The five IASs create a 'box' around the magnesium atom, which limits its volume. In principle, its atomic basin extends to infinity but the IASs virtually touch each other as they move towards infinity. Hence, for practical purposes the Mg ion is topologically closed, the way it would be in a crystal but then without the protruding ''wings''.

3.3. [18]Annulene

In Fig. 8, we show the IASs bounding one carbon atom and the IASs bounding one inner hydrogen atom in the [18]annulene molecule. The 18 carbons are part of an aromatic ring and of course connected by covalent bond paths. More remarkably, the six inner hydrogen atoms are also connected by bond paths and form a six-membered ring. This feature is reminiscent of recent work by Matta et al. [35] on phenanthrene, chrysene, dibenz[*a*,*j*]anthracene, planar biphenyl and other hydrocarbons. From the surfaces, it is clear to see that the aromatic carbons are actually each part of one or two six-membered rings with the inner hydrogens. Topologically, this example shows how the algorithm can handle multiple RCPs and curved ring lines. Note that this picture may give the false impression surfaces of constant electron density might have been added at the top of both atoms. We emphasize that this is not the case.

3.4. Adamantane

Adamantane or tricyclo(3,3,1,1)decane is a classic example of a regular molecule with a cage critical point.

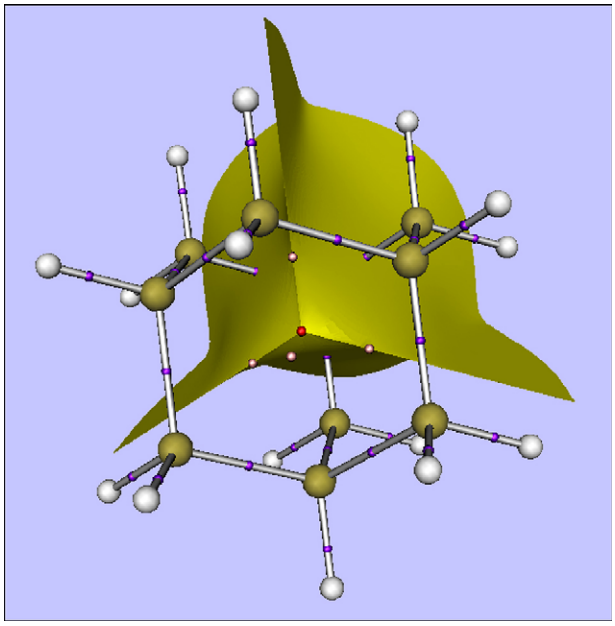

Fig. 9. A tertiary carbon in adamantane. The carbon nuclei are shown in gold and the hydrogens in white. The bond paths are represented by the grey solid lines, the bond critical points by purple spheres, the ring critical point by pink spheres and the cage critical point by a red sphere.

We have triangulated the surfaces of one of the tertiary carbons, as shown in Fig. 9. The cage is surrounded by four (topological) rings. All C–C IASs are limited by two ring lines and the cage critical point. Once again the algorithm is able to manage these topological difficulties.

3.5. Water cluster

Water clusters have a very complicated topology. The intermolecular hydrogen bonds create many ring and cage critical points. In this example, we studied a geometry-optimized nonamer, shown in Fig. 10. The bond paths in Fig. 10a demonstrate that the water molecules are arranged in a kind of deformed cube. There are six rings, one on each side of the cube and one cage critical point in the middle of the cluster. The interatomic surfaces between the atoms are revealed in Fig. 10b.

3.6. Ferrocene

Ferrocene is a classic organometallic in which the iron atom is sandwiched between two cyclopentadiene rings. As shown in Fig. 11, the central iron atom is topologically very interesting because it is bonded to every carbon atom. Two subsequent carbons of the same aromatic ring form a three-membered ring with the iron atom displaying a curved ring line. Furthermore, there is a cage critical point between the iron and each aromatic ring. Also, the Fe–C IASs have a very high ellipticity ($\varepsilon = 0.88$). Despite all these challenges, the algorithm performs well and correctly triangulates every IAS.

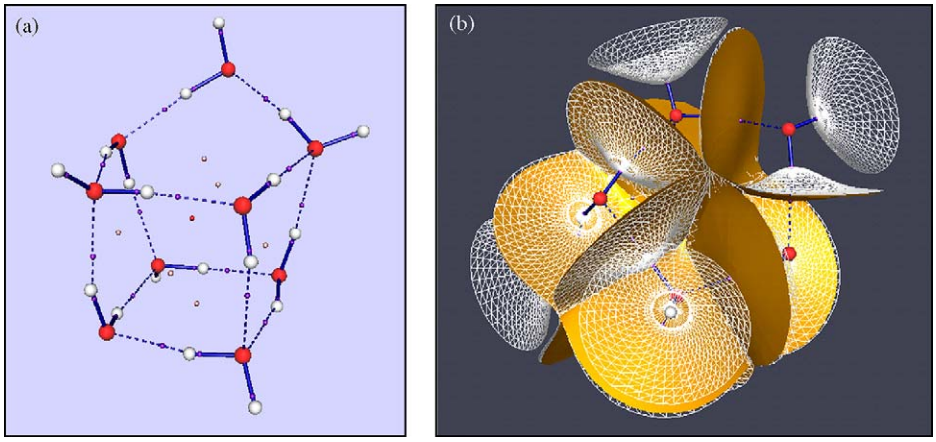

Fig. 10. (a) Bond paths in a water nonamer. Intramolecular (covalent) bond paths (blue) link oxygen nuclei (red) and hydrogen nuclei (white). Intermolecular interactions are marked by plain blue lines. The bond critical points are in purple, the ring critical points in pink and the cage critical point in red. (b) Surfaces of the intramolecular O–H interactions (in white wireframe) and intermolecular O–H interactions (solid, in orange) of the water nonamer. The nuclei, bond paths and critical points are shown in the same way as in Fig. 9a.

3.7. Tuftsin

Tuftsin [36] is the tetrapeptide ThrLysProArg. It originates from human immunoglobulin G and possesses analgesic properties. Fig. 12a shows a complicated network of bond paths as expected in oligopeptides and even more so in proteins. Curious C–H···H–C interactions are reminiscent of stabilizing interactions in citrinin [1]. Fig. 12b shows a peptide group as the first example of a functional group.

3.8. Nucleotide

In the final example, we triangulated several IASs appearing in the dCpdG dinucleotide, in which a single phosphate group links two deoxynucleosides, cytidine and guanosine. The overall pattern of bond paths is shown in Fig. 13a. The two nucleosides interact with three hydrogen bonds (bottom left). They appear again more clearly in

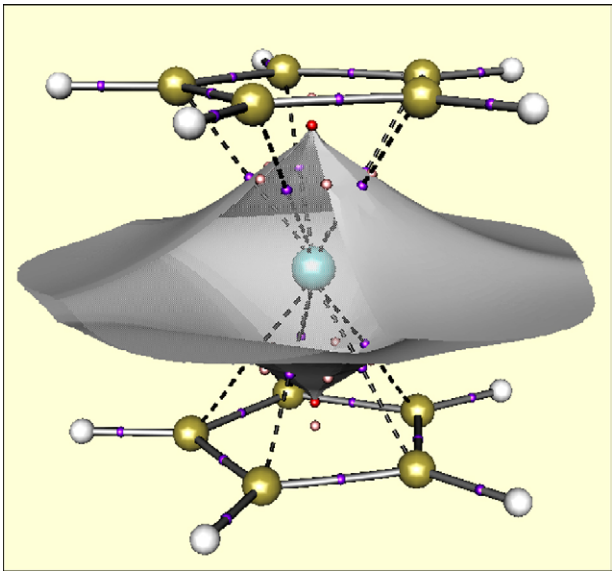

Fig. 11. The iron atom (IASs in grey) in the ferrocene complex. The IAS at the left front is transparent. The iron nucleus is in blue, the carbons in gold, and the hydrogens in white. The covalent bond paths are the grey solid lines, the non-covalent ones are the black dashed lines. The bond critical point is shown in purple, the ring critical point in pink and the cage critical point in red.

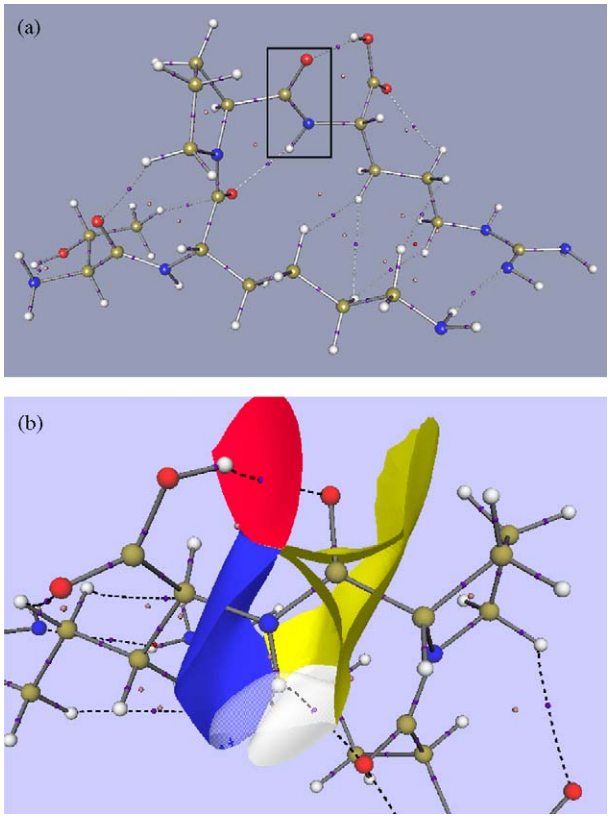

Fig. 12. (a) Bond paths in the tetrapeptide tuftsin (ThrLysProArg). The carbon nuclei are in gold, the oxygens in red, the nitrogens in blue and the hydrogens in white. The covalent bond paths are the grey solid lines, the non-covalent ones are the black dashed lines. The bond critical point is shown in purple, the ring critical point in pink and the cage critical point in red. (b) A close-up of the peptide group (HNC═O) corresponding to the boxed area in Fig. 11a.

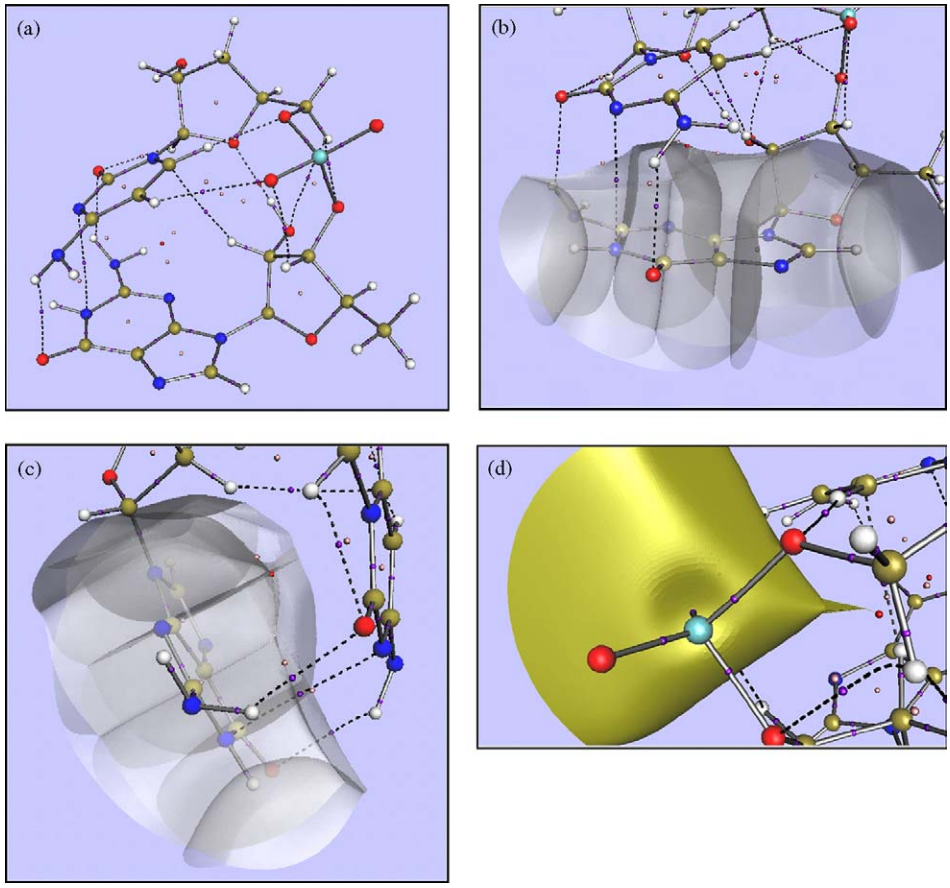

Fig. 13. (a) Patterns of bond paths in dCpdG. The nuclei are C (gold), O (red), N (blue), H (white) and P (cyan). Covalent bond paths (grey solid lines), the non-covalent ones (dashed lines). Bond critical point (purple), ring critical point (pink) and cage critical point (red). (b) Semi-transparent IASs (grey) bounding the atoms of the guanine base. (c) Same object as in Fig. 12b but different view. (d) Oxygen of the phosphate group bounded by golden IASs. Note the narrow funnel-like structure reaching out to the cage critical point.

Fig. 13b and c where the IASs of guanine carve this fragment out of the dinucleotide. In Fig. 13d, we highlight a topological peculiarity: in one of the IASs bounding an oxygen atom of the phosphate group the GPs suddenly reach out to the nearby cage critical point, thereby creating a sharp spike in the surface.

4. Conclusion

The topology of the electron density offers a novel way to visualize atoms and bonds. Atomic properties such as multipole moments can be associated with this visual representation of atoms. Quantum chemical topology enjoys the benefit of *visual representation going hand in hand with physical property*, and the benefit that it is based on the electron density itself, rather than on the way it was obtained. The outlined algorithm is able to deal with complex topologies occurring in larger systems. As an added bonus the algorithm solves a long-standing problem of gaps appearing in interatomic surfaces. This opens a new avenue to robust and faster atomic integration.

References

[1] P.L.A. Popelier, in: D.J. Wales (Ed.), Structure and Bonding. Intermolecular Forces and Clusters, Springer, Heidelberg, Germany, 2005.
[2] B.T. Sutcliffe, Int. J. Quant. Chem. 58 (1996) 645–655.
[3] B.T. Sutcliffe, Int. J. Quant. Chem. 90 (2002) 66–79.
[4] R.G. Woolley, J. Am. Chem. Soc. 100 (1978) 1073–1078.
[5] P.L.A. Popelier, M. Devereux, M. Rafat, Acta Cryst. A60 (2004) 427–433.
[6] R.F.W. Bader, Atoms in Molecules. A Quantum Theory, Oxford University Press, Oxford, GB, 1990.
[7] P.L.A. Popelier, Scientific Computing World (1999) 26–28.
[8] R.F.W. Bader, in: P. van R. Schleyer (Ed.), Encyclopaedia of Computational Chemistry, vol. 1, Wiley, Chichester, GB, 1998.
[9] P.L.A. Popelier, Atoms in Molecules. An Introduction, Pearson, London, Great Britain, 2000.
[10] P.L.A. Popelier, P.J. Smith, in: A. Hinchliffe (Ed.), Chemical Modelling: Applications and Theory, vol. 2, Royal Society of Chemistry Specialist Periodical Report, 2002, pp. 391–448 (Chapter 8).
[11] P.L.A. Popelier, F.M. Aicken, S.E. O'Brien, in: A. Hinchliffe (Ed.), Chemical Modelling: Applications and Theory, vol. 1, Royal Society of Chemistry Specialist Periodical Report, 2000pp. 143–198 (Chapter 3).
[12] R.F.W. Bader, Phys. Rev. B 49 (1994) 13348–13356.
[13] P.J. MacDougall, C.E. Henze, Theor. Chem. Acc. 105 (2001) 345–353.

[14] M. Kohout, Chemical Bonding Analysis in Direct Space, 2002 http://www.cpfs.mpg.de/ELF.
[15] M. Kohout, Programs DGrid and Basin, 2005 http://www.scm.com/News/DGrid.html.
[16] N. Malcolm, R.J. Gillespie, P.L.A. Popelier, Dalton Trans. (2002) 3333–3341.
[17] B. Silvi, A. Savin, Nature (London) 371 (1994) 683–686.
[18] B. Silvi, C. Gatti, J. Phys. Chem. A 104 (2000) 947–953.
[19] C. Gatti, A. Volkov, Program TOPXD, 2001, http://harker.chem.buffalo.edu/public/topxd.
[20] V. Luana, Program TESSEL 2.0, 1996, http://web.uniovi.es/qcg/tessel/tessel.html.
[21] R.B. Corey, L. Pauling, Rev. Sci. Instrum. 24 (1953) 621.
[22] M.L. Connolly, Science 221 (1983) 709.
[23] P.L.A. Popelier, F.M. Aicken, J. Am. Chem. Soc. 125 (2003) 1284–1292.
[24] A.M. Pendas, V. Luana, L. Pueyo, E. Francisco, P. Mori-Sanchez, J. Chem. Phys. 117 (2002) 1017–1023.
[25] A.M. Pendas, V. Luana, J. Chem. Phys. 119 (2003) 7643–7650.
[26] P.L.A. Popelier, Can. J. Chem. 74 (1996) 829–838.
[27] P.D. Walker, P.G. Mezey, J. Am. Chem. Soc. 116 (1994) 12022–12032.
[28] F.W. Biegler-Koenig, R.F.W. Bader, T.H. Tang, J. Comp. Chem. 3 (1982) 317–328.
[29] P.L.A. Popelier, Comp. Phys. Commun. 108 (1998) 180–190.
[30] N.O.J. Malcolm, P.L.A. Popelier, J. Comput. Chem. 24 (2003) 1276–1282.
[31] P.L. George, F. Hecht, E. Saltel, Comp. Meth. Appl. Mech. Eng. 92 (1991) 269–288.
[32] N. Amenta, M. Bern, Discrete Comput. Geom. 22 (1999) 481–504.
[33] S.W. Sloan, Comp. Struct. 47 (1993) 441–450.
[34] P.L. Chew, ACM 87 (1987) 215–222.
[35] C.F. Matta, J. Hernandez-Trujillo, T.-H. Tang, R.F.W. Bader, Chem. Eur. J. 9 (2003) 1940–1951.
[36] S.D. O'Connor, P.E. Smith, F. Al-Obeidi, B.M. Pettitt, J. Med. Chem. 35 (1992) 2870–2881.